JOURNAL OF PROPULSION AND POWER
Vol. 14, No. 3, May–June 1998

Heat Transfer in Counterswirled Coaxial Jet Mixing

J. L. Sanger*
Woodworker's Supply, Casper, Wyoming 82061
and
P. A. Dellenback†
University of Wyoming, Laramie, Wyoming 82071-3295

Convective heat transfer data are presented for the mixing of two counterswirled coaxial jets confined by a constant-diameter tube. The inner jet Reynolds number was 3×10^4, its swirl number was 1, and its diameter was approximately twice the annular gap dimension. Annular jet swirl numbers varied from 0 to 1.2. Annular flow rates were characterized by a ratio of annular-to-inner jet axial momentum (denoted by MFR), which was varied from 0 to 8.2. Plots of local Nusselt numbers show minimums and maximums corresponding to the separation and reattachment points associated with wall-bounded recirculation cells. Local heat transfer coefficients were found to be a strong function of streamwise position and annular swirl number at low values of MFR, yet at high values of MFR, there is minimal streamwise variation in heat transfer coefficient as the mean flow largely dictates heat transfer rates. The product of MFR and annular swirl number is shown to be a key parameter in describing heat transfer enhancement downstream of wall-bounded recirculation cells. Several quantitative results should be useful to gas turbine combustor design efforts.

Nomenclature

C_t = Craya–Curtet number, $U_m/[(U_i^2 - U_a^2)(d/D)^2 + 0.5(U_a^2 - U_m^2)]^{1/2}$, where $U_m = (U_i - U_a)(d/D)^2 + U_a$
D = diameter of annular jet and mixing region
D_H = hydraulic diameter
d = diameter of inner jet
d_o = outside diameter of tube confining inner jet
f = friction factor for fully developed turbulent pipe flow
k = thermal conductivity of water
Nu = local Nusselt number
Nu_G = fully developed Nusselt number for turbulent tube flow computed from the Gnielinski[14] correlation
Pr = Prandtl number
q = local heat flux
R = radius of the test section
Re = Reynolds number of the inner jet based on U_i and d
Re_D = local Reynolds number in mixing region based on total bulk velocity, D, and local bulk temperature
r = radial position in tube relative to centerline
S = swirl number of jet upstream of mixing region, defined by $2\int_{R_2}^{R_1} r^2 uv\, dr/D_H \int_{R_2}^{R_1} ru^2\, dr$, where for inner jet, $R_1 = 0$ and $R_2 = d/2$, and for annular jet, $R_1 = d_o/2$ and $R_2 = D/2$
T_b = bulk fluid temperature
T_w = inside tube wall temperature
U = bulk axial velocity
u = local axial velocity
v = local circumferential velocity
X = axial distance from location where jets begin mixing

Subscripts
a = annular jet
i = inner jet

Received Jan. 17, 1997; revision received Dec. 17, 1997; accepted for publication Dec. 17, 1997.

*Director of Engineering, Research and Development.
†Associate Professor, Department of Mechanical Engineering.

I. Introduction

SWIRL has long been utilized as a means for enhancing turbulent mixing and convective heat transfer.[1] These two features acting in unison are not always attractive, as for example in gas turbine combustor applications where the vigorous mixing is attractive, but the augmented heat transfer is not. In addition to enhancing mixing, another important motivation for incorporating swirl in combustors is that for sufficiently high swirl levels, a stable on-axis recirculation region is formed that provides a mechanism for flameholding. The on-axis recirculation arises when the circumferential velocity component decays in the streamwise direction, resulting in a corresponding increase in pressure that provides the adverse pressure gradient necessary to drive the recirculation.[2] Other recirculation cells may also be present in simulated combustor flows. For example, in confined coaxial jet mixing, differences in jet velocities can result in a recirculation zone lying adjacent to the tube wall.[3,4] Finally, some combustor designs that have been motivated by a desire to achieve extremely intense mixing rates have surrounded a central swirling jet with a second coaxial jet swirled in the opposite direction, thus providing very high levels of circumferential shearing with accompanying turbulence generation.

The purpose of the present investigation was to support prior flowfield studies through an experimental examination of the convective heat transfer in counterswirled coaxial jet mixing confined by a constant-diameter tube. While on-axis recirculation has been well documented because of its importance as a flameholding mechanism, wall-bounded recirculation, which is clearly an important feature in the convective heat transfer problem, has received relatively little attention. Thus, the location and extent of the wall recirculation zone (whose reattachment point results in a hot spot) was of particular interest in the present study. In the present experiments, the existence of a wall-bounded recirculation region has been inferred from local heat transfer measurements. An important goal of the investigation was to provide guidance for combustor designers, who are concerned with protecting combustor-liner walls from excessive heat loads by examining the roles of jet flow ratios and swirl strengths on the heat transfer process.

Prior investigations of counterswirled coaxial jet mixing have examined velocity fields in axisymmetric expansions, di-

verging cross sections, and in constant-diameter tubes. Because of space limitations and the significant differences between sudden expansion and constant-diameter-tube flowfields, only prior investigations associated with the latter geometry will be summarized here. Various investigations[5–8] have reported on aspects of counterswirled coaxial jet mixing in a constant-diameter tube. Vu and Gouldin[5] found that the outer swirl had a strong effect on the formation of an on-axis recirculation region and on mixing characteristics in the shear layer. As the magnitude of the annular swirl was varied from their maximum counterswirl to maximum coswirl conditions, the diameter and length of the on-axis recirculation region diminished. The principle factor in recirculation-cell size was thought to be the level of turbulence generated by the inner jet shearing. No wall-bounded recirculation was observed, probably because of the high values of annular jet velocity employed in their experiments.

An investigation by Gouldin et al.[6] used a laser Doppler anemometer (LDA) to measure velocities in a model combustor with a jet diameter ratio d/D of 0.5, a velocity ratio U_i/U_a of 1.4, an inner jet swirl number S_i of 0.50, and annular jet swirl number S_a of ± 0.56, i.e., both coswirl and counterswirl. The authors concluded that turbulent transport was not the mechanism for swirl-induced on-axis recirculation. Rather, they suggested that formation of an on-axis recirculation region is an inviscid flow process only indirectly influenced by viscous and turbulent momentum transport.

Measurements in isothermal coaxial jet mixing were made by Ramos and Somer[7] using an LDA in a model combustor with a d/D of 0.26. A velocity ratio U_i/U_a of 1.5 and swirl numbers of $S_i = 0.58$ and $S_a = 0.54$ were examined. On-axis recirculation zones were documented for both coswirl and counterswirl conditions. Experimental data agreed satisfactorily with computational modeling, but not with coswirl data obtained in other investigations. This discrepancy was attributed to differences in geometry between experiments.

Sukhovich[8] investigated temperature distributions in coaxial jets where the inner jet was comprised of a high-temperature, unswirled gas. A swirled annular jet was maintained at lower temperatures. For jet diameter ratios of $d/D = 0.74$ and 0.41, Sukhovich found that centrifugal forces produced by swirled flows promote stable temperature stratification of the flow and significantly reduce heat fluxes to the tube wall. Increasing the strength of annular swirl reduced the gas temperature near the mixing tube wall while simultaneously increasing the local heat transfer. Sukhovich concluded that swirled films of cool gas could be used for effective protection of combustor walls against excessive temperatures.

II. Experimental Apparatus

The central element of the test facility was a recirculating water flow loop, as depicted in Fig. 1. Swirl was imparted to the 5.08-cm-diam inner jet with tangential slot generation. Details of the inner jet swirl generator construction are available in Dellenback et al.[9] Termination of the inner tube (that point at which mixing of the two jets began) was 16 inner jet diameters (or $8D$) downstream of the tangential slots, providing a substantial length for flow development of the inner jet.

Swirl was introduced into the annular jet, opposite the direction of inner jet swirl, by passing water through six 2.54-cm rigid tubes welded symmetrically and tangentially to the outside of a 9.98-cm-diam tube. The 9.98-cm-diam tube was concentric with the smaller tube containing the swirled inner jet. Annular swirl strength was varied by adjusting the relationship between the axial and tangential flow rates to the annular swirl generation device. The mixing region was located 20 annular gap spacings, i.e., $(D - d_o)/2$, or $5.5D$ downstream of the annular swirl generator to allow for flow development. The i.d. of the annular jet was 5.40 cm, whereas the o.d. of the annular jet was 9.98 cm. All flow rates were measured with turbine flow meters.

Heat transfer measurements were made in a horizontal stainless-steel tube by passing alternating current in the tube wall, thus producing a nearly uniform heat-flux boundary condition. Heating began at the same streamwise location where the two jets began mixing (Fig. 2). The heated test section had an i.d. of 9.98 cm, a wall thickness of 0.89 mm, and a length of 1.04 m. Stainless steel flanges were carefully attached to each end of the tube by very shallow welds at the extreme ends of the tube. Further details of the test-section construction are available in Dellenback et al.[10]

Conduction losses from the test section to the upstream tube were minimized by inserting a low-thermal-conductivity spacer (Melamine) between the two connecting flanges. The flanges and spacer were held together with nylon bolts to further minimize heat conduction to or from the test section. A plenum was installed downstream of the test section, also using a dielectric spacer and nylon bolts, to allow measurement of a bulk fluid temperature.

Electrical busses, machined from copper plate 1.27 cm thick, joined current-carrying cables to the stainless-steel flanges of the test section. Two water-carrying copper tubes were soldered around the periphery of the busses' outer rim for the purpose of guard heating or cooling. Each test section flange had a pair of thermocouples imbedded at different radial locations so that radial temperature gradients could be monitored and minimized through appropriate adjustment of water temperature to the outer rims of the guard heaters/coolers.

Temperatures on the exterior surface of the test section were measured with thermocouples mounted on the outside of the tube. Nineteen thermocouples were employed, spaced at smaller intervals near the upstream end of the test section to provide high-temperature resolution in the region of rapidly changing heat transfer coefficients. The Grashof number for the worst case in the present experiments was sufficiently low that free convection effects were entirely overwhelmed by forced convection according to the criteria presented by Metais and Eckert.[11] Prior studies[10] with the same equipment, but at

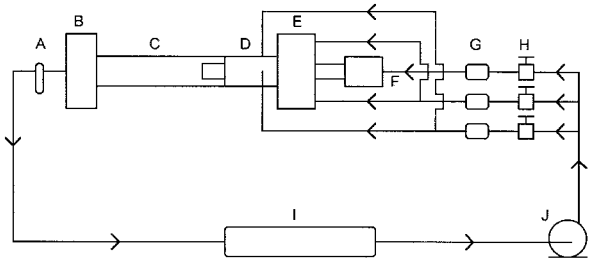

Fig. 1 Schematic of the water flow loop. A, filter; B, plenum; C, test section; D, annular swirl generator; E, annular flow plenum; F, inner jet swirl generator; G, flow meters; H, control valves; I, heat exchanger; J, pump.

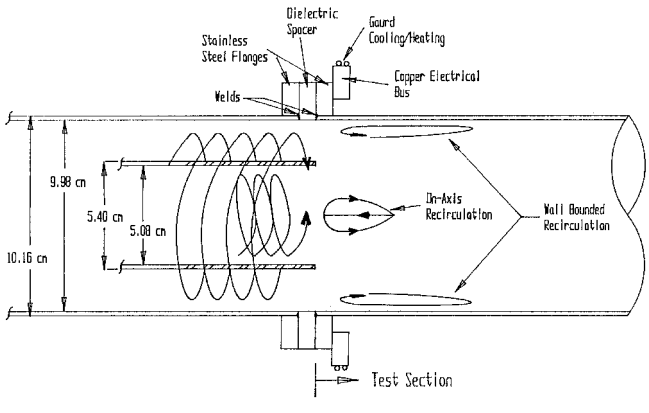

Fig. 2 Schematic of the test section and flow structure at the entrance to the mixing region.

even lower swirl levels, have confirmed that circumferential thermocouple position was unimportant to the results obtained. Thus, thermocouples were placed on the side of the test section as a matter of convenience. Finally, 13 cm of fiberglass insulation surrounded the test section, flanges, and the outer rim of the electrical busses.

Power input levels to the working fluid were deduced in two ways. In the first, power was taken as the product of the test-section resistance and the square of the current through the test section. Current through the test section was measured with a current transformer. Resistance of the type-321 stainless-steel test section was computed during the data-reduction process by taking account of the local temperature-dependent resistivities[12] along the test section.

Input power was also determined from the measured fluid enthalpy rise through the test section. To this end, bulk fluid temperatures were measured at the inlet and outlet of the test section with immersion thermocouples. For the data presented herein, the absolute discrepancy between the electrical power dissipated and the fluid enthalpy rise averaged 2.0% and was never more than 4.1% for any one run. The power dissipation was neither consistently larger nor smaller than the enthalpy rise, rather the discrepancies in power input appeared to be random.

III. Procedures and Data Reduction

Local heat transfer results are presented in terms of Nusselt numbers normalized with those for fully developed nonswirling flow, where

$$Nu = hD/k \tag{1}$$

k was evaluated at the local bulk temperature, and the local heat transfer coefficient was defined as

$$h = q/(T_w - T_b) \tag{2}$$

Bulk fluid temperatures ranged from 29 to 31°C, while typical temperature differences between T_w and T_b ranged from a low of 7°C near flow reattachment to a high of 29°C in the downstream region.

Although the present experiments had a nominally uniform heat-flux boundary condition (with a heat flux of about 4.5 W/cm^2), the local heat fluxes were not strictly uniform because of the temperature dependence of tube material properties and axial heat conduction in the tube wall. The procedure used for finding the local heat fluxes began by dividing the wall into 19 hypothetical control volumes centered on the locations of the 19 wall-temperature thermocouples. The magnitude of Joule heating in each volume was determined as the product of the control volume's temperature-dependent resistance and the square of the current. Heat loss from the outside of the tube wall through the fiberglass insulation that surrounded the test section was assumed negligible. This loss was calculated to be no more than 0.1% of the total power input in a worst-case analysis of the data. The heat conducted from one control volume to its neighbors was computed as a part of the data-reduction process and used to correct the local heat flux for each control volume. The data revealed that, at most, the axial heat conducted from one control volume to another represented 0.3% of the total heat generated in that volume.

The T_w in Eq. (2) is the temperature of the inside surface of the test-section wall. Because exterior surface temperatures were actually measured, the interior surface temperatures were determined from solution of the one-dimensional heat conduction equation for a cylindrical shell.[13]

Because the local heat flux and inside tube wall temperature were functions of each other, their determination was inherently an iterative process, but one that converged in one or two iterations because the temperature differences across the thickness of the tube wall were small (typically on the order of 1°C). For the worst case in the present experiments, the maximum variation in local heat flux between any two locations on the tube was calculated during the data-reduction process to be less than 2.3%. However, the extreme variations in heat flux for other cases were typically less than 0.5%, and the difference in heat flux between any two adjacent control volumes was less than 0.5% for all cases. Finally, to be consistent in methodology, local bulk temperatures were computed adjacent to each of the 19 control volumes from an energy balance that considered the local, slightly nonuniform heat input for each control volume.

Nusselt numbers for fully developed turbulent flow were determined from the Gnielinski correlation,[14] which Kakac et al.[15] recommend as probably the best available general-purpose correlation:

$$Nu_G = (f/2)(Re_D - 1000)Pr/[1 + 12.7(f/2)^{0.5}(Pr^{0.667} - 1)] \tag{3}$$

The friction factor that appears in Eq. (3) was evaluated from the Techo et al.[16] correlation, again recommended by Kakac et al:

$$f = \left(1.7372\ \ell n\{Re_D/[1.964\ \ell n(Re_D) - 3.8215]\}\right)^{-2} \tag{4}$$

All fluid properties used in Eqs. (3) and (4) were evaluated at the local bulk temperature.

The method of Kline and McClintock[17] was employed to determine that the largest uncertainties were about 2% in inner jet Reynolds number and momentum flux ratio and 8% in swirl number. The largest uncertainties in Nusselt number were computed to be about 9%, with these occurring near the location of peak Nusselt number where wall-to-bulk temperature differences were smallest.

IV. Results and Discussion

The Prandtl number of the fluid entering the heated test section was 5.5 ± 1% throughout the series of experiments. The inner jet Reynolds number of 3×10^4 (±0.5%) was based on inlet bulk fluid properties and the bulk axial velocity in the upstream tube. The inner jet swirl number was computed from the results of Dellenback et al.,[9] who measured velocity profiles with an LDA for the same inner jet swirl generator and inlet sections used in the present experiments. The velocity measurements were made one mixing tube diameter D upstream of the mixing region.

While the Craya–Curtet number[3] has proven suitable for correlating data in past investigations of coaxial jet mixing, it is undefined at the larger annular-to-inner jet velocity ratios examined in the present study, i.e., for $U_a/U_i > 1$. Thus, a ratio of axial momentum fluxes was used to characterize the annular flow rate. The ratio of annular-to-inner jet streamwise momentum flux $\dot{m}_a U_a/\dot{m}_i U_i$ is denoted by the acronym for momentum flux ratio, or MFR. In the present experiments, the MFR was related to velocity ratios, Reynolds number ratios, and to the Craya–Curtet number through the geometry of the jets as shown in Table 1.

A. Summary of the Flowfield

Axial and circumferential mean velocity profiles and distributions of turbulence intensity are available for the inner jet,

Table 1 Relationship between various parameters for characterizing the annular flow

MFR	0	0.37	1.46	2.77	8.30
U_a/U_i	0	0.37	0.73	1.00	1.74
C_t	0.55	1.38	3.08	N/A	N/A
Re_a/Re_i^a	0	0.33	0.66	0.90	1.57

[a] Re_a is based on the hydraulic diameter of the annular jet ($D_H = D - d_o$).

upstream of the mixing region, in Dellenback et al.[9] To characterize the annular jet and determine its swirl number, axial and circumferential velocities were measured with an LDA one diameter D upstream of the mixing region for four values of MFR and three values of annular swirl number. Various and arbitrary ratios of tangential-to-axial flow rates (here called FR, for flow ratio) were supplied to the annular swirl generator, velocity measurements were then made, and swirl numbers computed. Figure 3 shows the relationship between FR and the annular swirl number S_a that resulted. The data in Fig. 3 are independent of the MFR and can be described to within $\pm 4\%$ for $0 < S_a < 1.4$ with the simple relationship

$$S_a = 1.41\mathrm{FR}^{1.90} \tag{5}$$

Equation (5) represents an extensive number of LDA measurements, and it is included here as a possible aid in designing or characterizing other swirl generation devices.

Both axial and circumferential components of mean and rms velocities were normalized with the annular bulk velocity for each MFR. These velocities were 0.19 m/s for MFR = 0.37, 0.38 m/s for MFR = 1.46, 0.53 m/s for MFR = 2.8, and 0.90 m/s for MFR = 8.2. Figure 4 shows that as the annular swirl strength was increased, the location of the maximum circumferential velocity moved from the o.d. to the midregion of the annular jet. Figure 4 also shows that the magnitudes of axial velocity tended to remain fairly constant for any swirl strength. However, as the swirl strength in the annulus increased, the

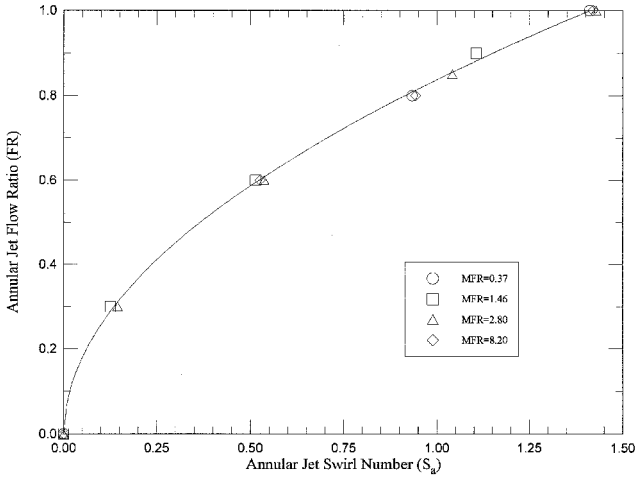

Fig. 3 Relationship between the annular jet swirl number and axial-to-tangential flow rate ratio supplied to the annular jet swirl generator.

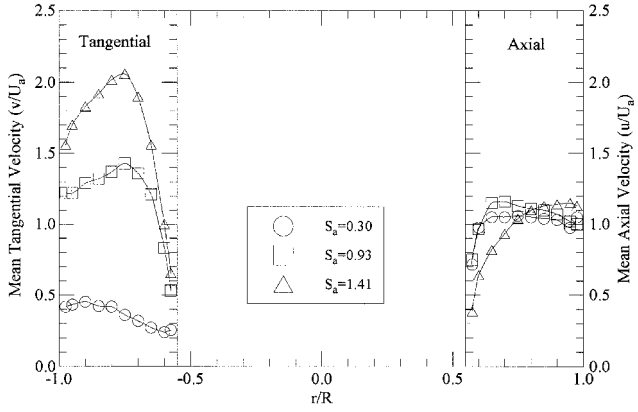

Fig. 4 Mean axial and tangential velocities for the annular jet, upstream of the mixing region ($X/D = -1.0$, MFR = 0.37, various S_a).

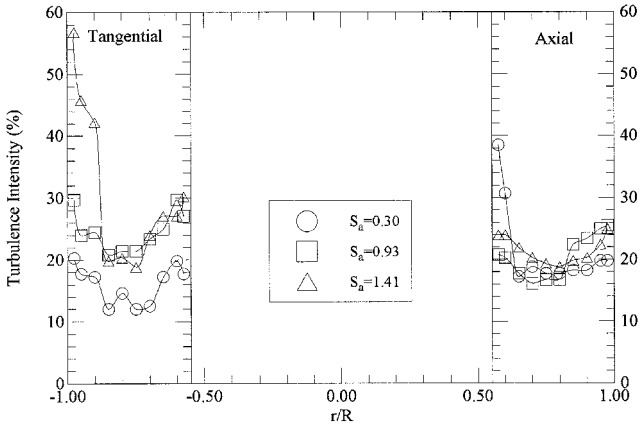

Fig. 5 Axial and tangential turbulence intensities for the annular jet, upstream of the mixing region ($X/D = -1.0$, MFR = 0.37, various S_a).

locations of maximum axial velocity shifted from smaller to larger radii in the annular jet. This shift was consistent with well-known trends in confined swirling flows.[10]

Hendricks and Brighton[18] found that inlet values of turbulent kinetic energy had a significant effect on the distribution of mean velocity in their coaxial jet mixing studies. Thus, rms velocities just upstream of the mixing region are presented in Fig. 5 to further document the inlet boundary condition. As the annular swirl strength increased, the magnitudes of turbulence intensity increased as shearing between the jets became more intense. The circumferential and axial turbulence intensities were between 15 and 30% except near the outer tube wall for the highest swirl number, where circumferential values were somewhat higher. The inner jet turbulence intensities were also between 15 and 30% one diameter D upstream of the mixing region.[9] To put these inlet values in perspective, note that Gouldin et al.[6] reported rms fluctuations peaking at about 60% (using annular bulk velocity for normalization of rms velocity) in the mixing region of counterswirled jets having swirl numbers of about 0.5.

B. Heat Transfer Results

The flows examined in the present investigation contain several common features that govern the heat transfer behavior. To gain some insight into what should be expected, it is useful to consider the limiting case of swirling flow through a sudden expansion that is similar to the present flows having a very low annular flow rate, i.e., as MFR $\rightarrow$ 0. The sudden expansion flows possess a wall-bounded recirculation region and a reattachment point where the jet flow expands to meet the wall downstream of the expansion. Convective heat transfer coefficients adjacent to the recirculation region are quite high[10] because of high turbulence levels associated with shearing as the jet expands into the larger downstream tube, and this occurs even though mean velocities in the recirculation cell are relatively low.[9] The heat transfer coefficient has a sharp peak near the point of flow reattachment and decreases downstream as the flow develops, consistent with usual explanations of developing-flow heat transfer. As the annular flow rate, or MFR, is increased from zero in the present experiments, it can be expected that the recirculation cell will be shifted and stretched in the downstream direction. The annular flow can also be expected to provide a film-cooling effect that will reduce the convective heat transfer. However, as the annular flow is swirled, the shearing between counterswirling inner and annular jets will increase, resulting in higher turbulence levels that will act to increase the wall heat transfer. Turbulence generation can also be significantly augmented by axial shearing when the axial velocities of the two jets are different. Thus, the present flows contain several competing effects that influence the heat transfer, and the results that follow have been

organized in terms of parametric variations to help understand the relative importance of the various flow processes.

Figure 6 shows the impact of annular swirl strength on the convective heat transfer and flow development at a single low value of MFR. Peak Nusselt numbers are slightly larger for the higher values of annular swirl number, and fully developed flow and heat transfer are approached somewhat more quickly as the annular swirl number is increased. Peak Nusselt numbers increase for increasing annular swirl number because shearing between the jets also increases, which results in higher levels of turbulent kinetic energy. Support for this argument is available from the measurements of Vu and Gouldin,[5] where turbulence intensities are 30% higher in a counterswirl configuration than in a coswirl configuration. However, that the Nusselt number should be smaller in the downstream region as S_a increases is perhaps surprising. This feature will be discussed later in this paper.

Table 1 shows that the bulk axial velocity of the inner jet is larger than that of the annular jet for MFR < 2.8. If entrainment of the annular jet is particularly efficient in the shear layer between the two jets, mass conservation will require that a recirculation cell be formed, usually near the tube wall where axial velocities are smallest.[3,4] The recirculation cell has a stagnation point at the tube wall that results in a peak in the heat transfer coefficient and a separation point at the wall where a minimum in the heat transfer coefficient will occur (see Fig. 2). Wall-bounded recirculation regions in constant-diameter tubes have not been documented by prior velocity measurements as far as the authors know, presumably because these regions are so thin that they are susceptible to alteration by conventional probes, and optical measurements near walls tend to be greatly hampered by light flare at the wall.

The annular swirl number has no significant influence on the location of the stagnation point (where the Nusselt number is a maximum), or on the location of the separation point, at low MFR. While no minimum in Nusselt number can be discerned in Fig. 6, it is presumed to lie upstream of $X/D = 0.2$, where interference with test section flanges precluded installation of thermal instrumentation. Extrapolation of the curves in Fig. 6 suggests that the annular swirl number also has a minimal impact on the location of the Nusselt number minimums. Thus, the size and location of the wall-bounded recirculation cell does not seem to be much affected by the strength of the annular swirl, at least for low values of MFR.

For contrast to the present data, Fig. 6 also shows the normalized Nusselt number for the related case of sudden expansion flow[10] for an inner jet Reynolds number of 3×10^4, an inner jet swirl number of 1, and tube diameters identical to those used in the present experiments. In contrasting the sudden expansion and coaxial jet data, it is clear that when the annular flow rate is low, the location of the peak Nusselt number is not altered significantly. The similarity in the distributions of the heat transfer coefficient suggests that the flow structures are similar in the two problems, but the film-cooling effect of the annular jet substantially reduces the heat transfer at all streamwise locations.

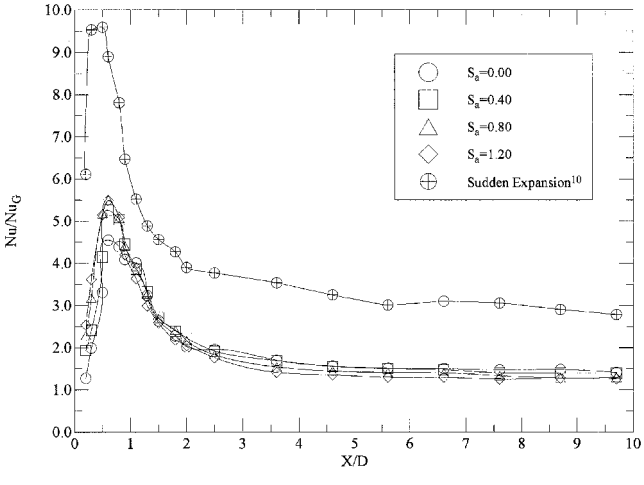

Fig. 6 Local Nusselt numbers for MFR = 0.37, various S_a, contrasted with sudden expansion data,[10] showing a significant film cooling effect even for low annular flow rates.

Figure 7 shows results for a higher annular flow rate having MFR = 1.46. With the increase in annular flow rate, the entire wall-bounded recirculation cell is shifted downstream, and the minimum in Nusselt number corresponding to the cell's separation point is captured in the data. The impact of the annular swirl number on the wall-bounded recirculation cell is also much more apparent at this larger MFR. As the swirl in the annular jet is increased, the reattachment point is shifted upstream, but the separation point is minimally affected and remains near $X/D = 0.5$. Hence, the axial length of the wall-bounded recirculation cell is compressed as the annular swirl is increased. Figure 7 shows that the maximum Nusselt number ratio also increases with increasing annular swirl number. This heat transfer enhancement is again caused by the increase in shearing and turbulence generation between the inner and annular jets.

Figure 8 shows the influence of annular swirl strength for an MFR = 2.80. Because this case corresponds to both jets having the same bulk axial velocities (Table 1), it is not surprising that there is little difference between maximum and minimum Nusselt numbers in the upstream region, suggesting only a very weak wall-bounded recirculation cell. As with MFR = 1.46, it is again clear that as the annular swirl strength

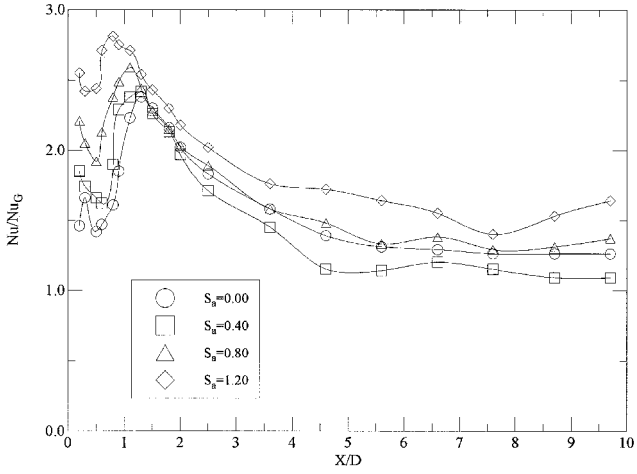

Fig. 7 Local Nusselt numbers for MFR = 1.46, various S_a

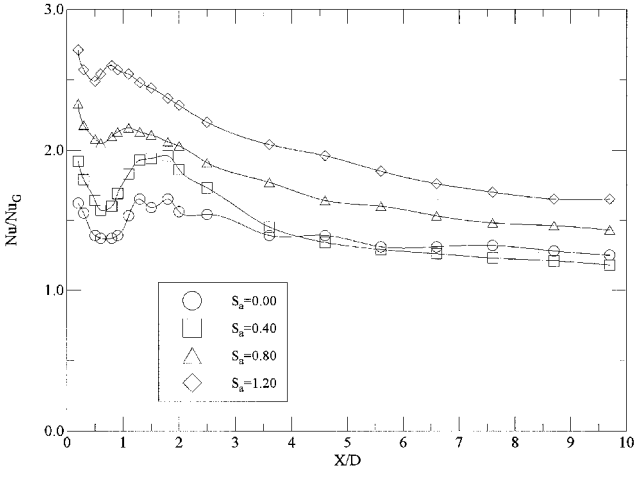

Fig. 8 Local Nusselt numbers for MFR = 2.80, various S_a

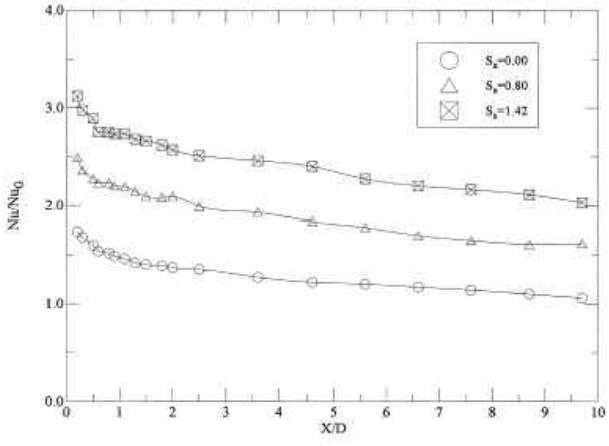

Fig. 9 Local Nusselt numbers for MFR = 8.20, various S_a

is increased, the recirculation cell is compressed and shifted upstream. Unlike the cases of lower MFR, the heat transfer coefficient is a fairly strong function of the annular swirl number at moderate levels of MFR. As Fig. 9 will help to show, with increasing annular flow rate, the influence of the mean flow appears to dominate the convective heat transfer problem while turbulent fluctuations play a lesser role.

The trend to annular flow dominance of heat transfer behavior is essentially complete for an MFR = 8.2, as shown in Fig. 9. Note that for MFR > 2.8, the annular mean velocity exceeds the mean inner jet velocity (Table 1). When the annular jet's bulk velocity is the larger of the two jet velocities, there is no mechanism for generation of wall-bounded recirculation cells, and any recirculation cells that may be induced should lie within the inner jet. Consistent with this hypothesis, we see no evidence of wall-bounded recirculation in the data of Fig. 9.

At large MFR, the principal effect of annular swirl is to increase the value of peak Nusselt number ratio in a uniform way. In fact, the Nusselt number ratio can be quantified as a function of annular swirl at large values of MFR. This relationship was determined to be

$$Nu/Nu_G = (Nu/Nu_G)_{Sa=0} \times (1 + S_a)^{0.72} \tag{6}$$

Equation (6) fits the data of Fig. 9 to within ±3.5% for $X/D > 1$.

C. Circumferential Momentum Ratio

There are results in Figs. 6–8 that require further consideration to explain the physical mechanisms governing the heat transfer. In particular, all three figures show that increasing the annular swirl number from 0 to 0.4 does not increase the downstream heat transfer, as might be expected. Because the two jets are swirled in opposite directions, each is tending to dissipate the circumferential momentum of the other. How long the swirl in each jet persists as it moves downstream is important because one of the primary mechanisms for heat transfer enhancement in the present flows is the high turbulent kinetic energy levels that arise from circumferential shearing. The decay of swirl in the jets can be related to a ratio of circumferential momentum for the two jets, and this quantity can then be used for explaining the interrelated effects of swirl and axial momentum flux in the earlier figures.

The rate of both inner and annular jet swirl decay should be some function of the initial circumferential momentum of the two counterswirled jets. The ratio of inner jet circumferential momentum to annular jet circumferential momentum can be shown to be a function of both swirl numbers and the momentum flux ratio by utilizing the definition of the swirl number

$$\frac{\text{circumferential momentum of inner jet}}{\text{circumferential momentum of annular jet}} = \frac{S_i \times \text{axial momentum of inner jet}}{S_a \times \text{axial momentum of annular jet}} \tag{7}$$

Because MFR = axial momentum annular jet/axial momentum inner jet, we have,

$$\frac{\text{circumferential momentum of inner jet}}{\text{circumferential momentum of annular jet}} = \frac{S_i}{S_a \times \text{MFR}} \tag{8}$$

The inner jet Reynolds number was 3×10^4 and the swirl number was 1.0 at the entrance to the mixing section for all data reported herein. Hence, the initial circumferential momentum associated with the inner jet was the same for all cases. However, the annular jet's circumferential momentum varied with both annular swirl number and momentum flux ratio. Equation (8) is a general definition, but to facilitate the explanation of Figs. 6–8, it has been plotted (Fig. 10) for the values of S_i, S_a, and MFR examined in the present study. There were three other combinations of S_a and MFR that were examined in the present investigation, but they are not shown in Fig. 10 because they exceed the arbitrary bounds chosen for the plot. Note that the curves in Fig. 10 are also asymptotic to two limits ($S_a \to \infty$ and $S_a = 0$).

In most flow situations, increasing swirl number results in increased heat transfer, but Figs. 6–8 have shown that this is not universally true when counterswirling jets are acting to dissipate each other. In fact, the shaded band in Fig. 10 represents the combinations of MFR and annular swirl number that result in downstream Nusselt numbers that are lower than those cases with no annular swirl. Thus, the crosshatched region of Fig. 10 identifies combinations of flow conditions that minimize downstream convective heat transfer, which would be attractive in combustor applications.

A simplified interpretation of Figure 10 is as follows. The circumferential momentum ratio indicates which jet's swirl will persist further downstream. For circumferential momentum ratios as defined by Eq. (8) near 1, we would expect that the two jets would relatively quickly dissipate each other's circumferential momentum and that downstream heat transfer would be low because of the absence of the important mechanism of circumferential shearing and turbulence generation. For circumferential momentum ratios larger than 1, the inner jet's circumferential velocity encounters only modest viscous

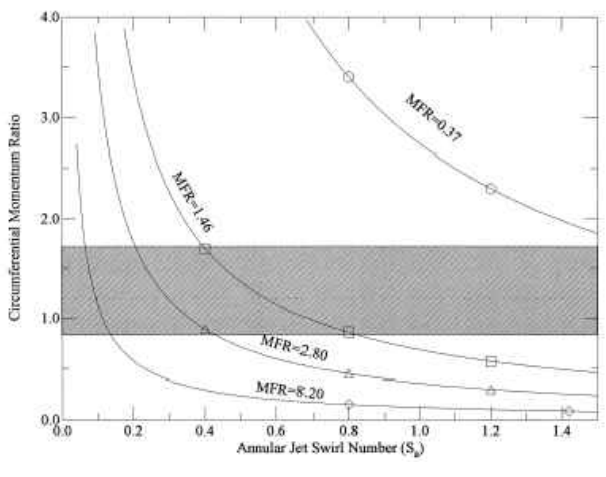

Fig. 10 Relationship between circumferential momentum ratio and S_a for MFRs examined in the present study.

resistance so that its swirl should persist further downstream than annular swirl. Similarly, for circumferential momentum ratios smaller than 1, the annular jet rapidly overwhelms the inner jet's circumferential momentum so that annular swirl will persist further downstream. For circumferential momentum ratios different from 1, circumferential shearing should remain an important mechanism driving heat transfer in the downstream region. This argument, although simple, is a useful starting point for explaining the interrelated effects of axial momentum and swirl and can be used to predict the effect of both on downstream heat transfer.

Recall that in Fig. 6, the downstream Nusselt numbers decreased as S_a increased. From the prior arguments, the annular jet's circumferential momentum was dissipated by the much higher circumferential momentum of the inner jet, so that while the inner jet swirl persisted into the downstream region, the mostly axial annular jet was acting to film cool the tube wall. For MFR = 0.37, Fig. 10 shows that the lower annular jet swirl numbers result in a very large imbalance in circumferential momentum, and even for the largest values of annular swirl number examined in the present study (S_a = 1.2), the inner jet circumferential momentum was dominant for this low MFR case. Apparently then, the heat transfer enhancement is largely a result of circumferential shearing and the resulting turbulent fluctuations.

The prior argument can also be used to interpret the downstream heat transfer in Figs. 7 and 8. Figure 7 showed that the S_a = 0 case had higher downstream Nusselt numbers than the S_a = 0.4 case for MFR = 1.46, and Fig. 8 showed similar Nusselt numbers for S_a = 0 and S_a = 0.4 when MFR = 2.80.

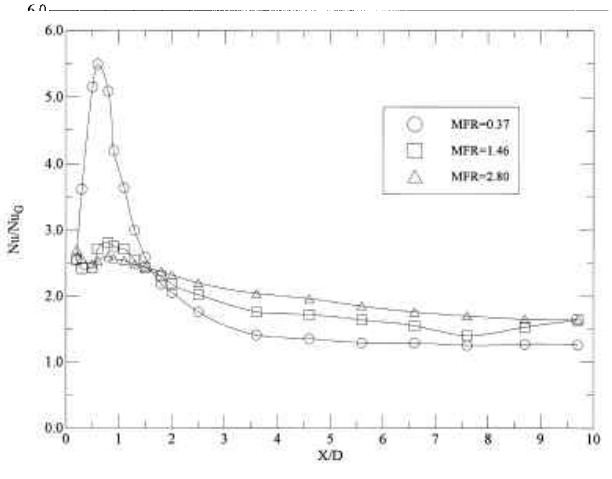

Fig. 11 Local Nusselt numbers for S_a = 1.2, various MFR.

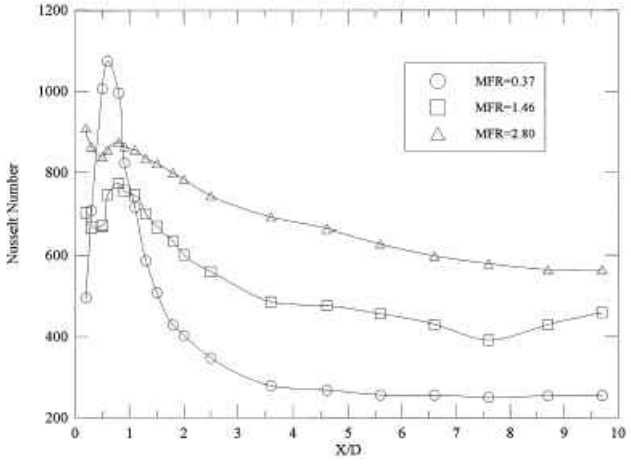

Fig. 12 Local Nusselt numbers for S_a = 1.2, various MFR.

In the two aforementioned cases where S_a = 0.4, the heat transfer was relatively low because the circumferential momentum ratios were near 1. Similarly, for the case with MFR = 1.46 and S_a = 0.8, the downstream heat transfer was similar to the S_a = 0 case because the circumferential momentum ratio was near 1, suggesting that little circumferential shearing was taking place in the downstream region. Finally, the downstream heat transfer augmentation evident in Fig. 9 (where MFR = 8.2) was most likely caused by large mean velocities associated with the annular jet's persistent circumferential velocity because the circumferential momentum ratio was much less than 1, and consequently little circumferential shearing was occurring.

Equation (8) shows that the circumferential momentum ratio is not only a function of the swirl strengths of the two jets, but also MFR. Figure 11 reiterates selected data from Figs. 6–8 with the goal of highlighting the effect of MFR. In Fig. 11, both S_i and S_a are constant. Because a normalized Nusselt number is being plotted, the effect of axial mean velocity (or *Re* number) should be normalized out of the data in the downstream region. However, the downstream Nusselt number ratios are clearly a function of MFR. At MFR = 0.37, this heat transfer enhancement is a result of circumferential shearing and turbulent fluctuations. At the two higher MFR, there remains significant circumferential shearing in which the annular jet has dominated (because the circumferential momentum ratios were much less than 1), and there is also a significant mean flow contribution to the heat transfer by the highly swirled annular jet. Other figures like Fig. 11 were generated for S_a = 0.4 and 0.8, and both the interpretations and conclusions were consistent with the preceding discussion.

Although the data between MFRs of 0.37 and 1.46 in Fig. 11 are perhaps too sparse for a definitive conclusion, they do suggest certain MFRs might be preferable, depending on the application. For example, in combustor applications where minimum heat transfer and a uniformly cool wall temperature are desirable, MFRs of 1.5 might represent minimally accepted values for design purposes to ensure minimization of hot spots and thermal gradients (resulting from wall-bounded recirculation) that obviously would occur for MFRs of 0.37 or lower. For those combustor designs that use the counterswirling jets configuration, circumferential momentum ratios near 1 will yield the lowest downstream Nusselt numbers.

Although there are attractions to using the Gnielinski correlation[14] for normalization of the Nusselt number, doing so can make extraction of Nusselt numbers or the heat transfer coefficient somewhat awkward. Consequently, Fig. 12 contains essentially the same data as Fig. 11, but has been included here to help put the magnitudes of the Nusselt number into perspective. Nusselt numbers, heat transfer coefficients, and all related measurements and results are tabulated in Sanger.[19]

V. Conclusions

In addition to the unique convective heat transfer data that have been presented for counterswirled coaxial jet mixing, there are several results that can be summarized:

1) For annular swirlers with both axial and tangential flow entry, the swirl number can be conveniently characterized as a function of readily measured flow rates to the swirler by Eq. (5).

2) For small-to-moderate momentum flux ratios (MFR < 2.8), a wall-bounded recirculation cell is present, resulting in sharp peaks in the Nusselt number distribution, i.e., wall hot spots.

3) For large MFR, the mean velocity dominates the heat transfer behavior and turbulent fluctuations appear to play only a minor role. The effect of annular jet swirl on the convective heat transfer can be quantified by Eq. (6) for large MFR.

4) A simple physical argument based on the ratio of circumferential momentum of the two jets has been advanced that is consistent with the present data and potentially useful as a tool

for predicting the impact of MFR and annular swirl strength on both the downstream ($X/D > 3$) heat transfer and the persistence of downstream swirl.

The practical importance of these results lies primarily in the design of gas turbine engine combustors where knowledge of the local Nusselt number is important to quantifying the local heat loads, which in turn govern how film-cooling holes and other cooling strategies should be designed.

References

[1]Razgaitis, R., and Holman, J. P., "A Survey of Heat Transfer in Confined Swirl Flows," *Future Energy Production Systems; Heat and Mass Transfer Processes*, edited by J. C. Denton and N. H. Afgan, Vol. 2, Hemisphere, New York, 1976.

[2]Gupta, A. K., Lilley, D. G., and Syred, N., *Swirl Flows*, Abacus Press, Cambridge, MA, 1984.

[3]Barchilon, W. D., and Curtet, R., "Some Details of the Structure of an Axisymmetric Confined Jet with Backflow," *Journal of Basic Engineering*, Vol. 86, Dec. 1964, pp. 777–787.

[4]Khodadadi, J. M., and Vlachos, N. S., "Experimental and Numerical Study of Confined Coaxial Turbulent Jets," *AIAA Journal*, Vol. 27, No. 5, 1989, pp. 532–541.

[5]Vu, B. T., and Gouldin, F. C., "Flow Measurements in a Model Swirl Combustor," *AIAA Journal*, Vol. 20, No. 5, 1982, pp. 642–651.

[6]Gouldin, F. C., Depsky, J. S., and Lee, S. I., "Velocity Characteristics of a Swirling Flow Combustor," *AIAA Journal*, Vol. 23, No. 1, 1985, pp. 95–102.

[7]Ramos, J. I., and Somer, H. T., "Swirling Flow in a Research Combustor," *AIAA Journal*, Vol. 23, No. 2, 1985, pp. 241–248.

[8]Sukhovich, Y. P., "Convective Heat Transfer in Turbulent Mixing of Bounded Coaxial Jets," *Heat Transfer-Soviet Research*, Vol. 11, No. 3, 1979, pp. 1–9.

[9]Dellenback, P. A., Metzger, D. E., and Neitzel, G. P., "Measurements in Turbulent Swirling Flow Through an Abrupt Axisymmetric Expansion," *AIAA Journal*, Vol. 26, No. 6, 1988, pp. 669–681.

[10]Dellenback, P. A., Metzger, D. E., and Neitzel, G. P., "Heat Transfer to Turbulent Swirling Flow Through a Sudden Axisymmetric Expansion," *Journal of Heat Transfer*, Vol. 109, Aug. 1987, pp. 613–620.

[11]Metais, B., and Eckert, E. R. G., "Forced, Mixed and Free Convection Regimes," *Journal of Heat Transfer*, Vol. 86, No. 2, 1964, pp. 295–297.

[12]*Thermophysical Properties of High Temperature Solid Materials, Vol. 3: Ferrous Alloys*, edited by Y. S. Touloukian, Thermophysical Properties Research Center, Purdue Univ., MacMillan, New York, 1967.

[13]Carslaw, H. S., and Jaeger, J. C., *Conduction of Heat in Solids*, Oxford Univ. Press, Oxford, England, UK, 1959.

[14]Gnielinski, V., "New Equations for Heat and Mass Transfer in Turbulent Pipe and Channel Flow," *International Chemical Engineering*, Vol. 16, No. 2, 1976, pp. 359–368.

[15]Kakac, S., Shah, R. K., and Aung, W., *Handbook of Single-Phase Convective Heat Transfer*, Wiley, New York, 1987.

[16]Techo, R., Tickner, R. R., and James, R. E., "An Accurate Equation for the Computation of the Friction Factor for Smooth Pipes from the Reynolds-Number," *Journal of Applied Mechanics*, Vol. 32, June 1965, p. 443.

[17]Kline, S. J., and McClintock, F. A., "Describing Uncertainties in Single-Sample Experiments," *Mechanical Engineering*, Vol. 75, Jan. 1953, pp. 3–8.

[18]Hendricks, C. J., and Brighton, J. A., "The Prediction of Swirl and Inlet Turbulence Kinetic Energy Effects on Confined Jet Mixing," *Journal of Fluids Engineering*, Vol. 97, March 1975, pp. 51–59.

[19]Sanger, J. L., "Heat Transfer and Flow Phenomena in Counter-Swirled Coaxial Jet Mixing," M.S. Thesis, Univ. of Wyoming, Laramie, WY, May 1993.